

Baryon spectroscopy at the LHCb experiment in $\Omega_c^0 \rightarrow \Omega^- \pi^+ \pi^- \pi^+$ decays

Author: Albert Casamitjana Formiga

Facultat de Física, Universitat de Barcelona, Diagonal 645, 08028 Barcelona, Spain.

Advisor: Carla Marín Benito and Lukas Calefice

Abstract: This project investigates the resonance spectrum of the Ω^- baryon through the decay $\Omega_c^0 \rightarrow \Omega^- \pi^+ \pi^- \pi^+$, using data from the LHCb Run 2. A dedicated selection was applied to suppress background and reconstruct Ω_c^0 candidates, and combining the DDL and DDD track categories, the signal yield was amplified. The *sPlot* method was used for background subtraction. The resulting $\Omega^- \pi^+ \pi^-$ mass spectra show differences between pion pairings, and the limited statistics prevent any firm interpretation.

Keywords: Particle physics, high energy physics, data analysis, strange particles, spectroscopy.

SDGs: Industry, innovation and infrastructure

I. INTRODUCTION

Understanding the baryon spectrum and identifying the missing baryon resonances are key challenges in hadron physics. In particular, the strange sector remains relatively unexplored compared to other sectors.

The spectrum of the Ω hyperon is one of the least known, and the properties of these particles and their excited states are still poorly understood. This gap highlights the need for dedicated experimental and theoretical efforts to explore the spectrum of the strange baryons and to search for the missing resonances that are predicted by current models.

This project aims to identify the excited states of the Ω^- baryon more effectively, by studying its resonance spectrum through the decay $\Omega_c^0 \rightarrow \Omega^- \pi^+ \pi^- \pi^+$, using data from the LHCb experiment.

Only four excited Ω^- states have been reported in experiments since the discovery of the ground state $\Omega(1672)$ at BNL in 1964 [1]. Three of them were observed in fixed-target experiments in the 1980s: $\Omega^-(2250)$ [2] [3], $\Omega^-(2380)$ [2], $\Omega^-(2470)$ [4]. More recently, in 2018, a fourth was discovered by the BELLE collaboration: $\Omega^-(2012)$ [5], and confirmed by the ALICE experiment [6]. Among the four excited Ω^- states, only the $\Omega^-(2470)$ has been observed so far through the same decay channel analyzed in this study.

II. LHCb

The Large Hadron Collider beauty experiment, or LHCb for short, is one of the four main experiments at the Large Hadron Collider (LHC) at CERN[10]. It is dedicated to heavy flavour physics, focusing on the decays and properties of bottom and charm hadrons. LHCb is specifically designed to study the abundant production of heavy-flavoured particles resulting from the proton-proton collisions at the LHC. Its main goals include precise studies of CP violation, investigations of rare decays, and the spectroscopy of heavy hadrons.

The LHCb detector is a single-armed forward spectrometer, which has a geometrical acceptance in the pseudorapidity region of $2 < \eta < 5$. This geometry is optimized for the detection of $b\bar{b}$ pairs, which are predominantly produced in the forward region.

There are two main classes of sub-detectors that make up the LHCb detector and work together to reconstruct and identify the particles produced: tracking detectors (VELO, TT, and tracking stations) and particle identification detectors (RICH, calorimeters, and muon chambers). When the particle interacts with the layers of the tracking system, it leaves signals that can be used to reconstruct its trajectory. By observing the curvature of the trajectory, caused by the magnetic field of a dipole magnet, the particle's momentum can be determined. In addition, the Vertex Locator (VELO) provides precise information about the position of the primary and secondary vertices (PV, SV).

Tracks that leave hits in all tracking detectors, including the VELO, are referred to as long tracks. They provide the best resolution in momentum and vertex reconstruction. In contrast, downstream tracks do not pass through the VELO and start only in the tracking stations. They typically arise from particles decaying outside the VELO and exhibit reduced resolution in momentum and vertex reconstruction.

Finally, Ring Imaging Cherenkov detectors (RICH) measure the particle's velocity using the Cherenkov effect, and when combined with the momentum, particles can be identified based on their mass.

Given the enormous amounts of collisions, LHCb relies on a trigger system that selects events of interest in real-time for storage and analysis. The system consists of a hardware trigger stage (L0) and two-stage software-based high-level trigger systems (HLT1 and HLT2), which combined reduce the data rate by several orders of magnitude, enabling efficient data collection and analysis.

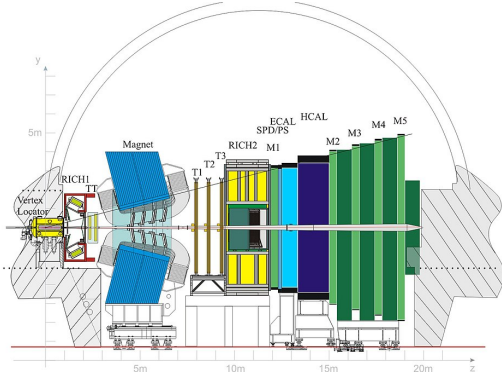


FIG. 1: Schematic side view of the LHCb detector, showing its main subdetectors.

A. Data set

The data used in this analysis consists of proton-proton collisions collected by the LHCb experiment during Run 2 (2016-2018), corresponding to an integrated luminosity of approximately 5.6 fb^{-1} .

Using the trigger system, the initial dataset is filtered to identify Ω^- particles. Further offline processing attempts to reconstruct Ω_c^0 candidates by combining reconstructed Ω^- baryons with three additional charged pions from the same proton-proton collision. However, since many pions are produced directly at the primary interaction point, this approach leads to a high rate of random combinations, introducing significant combinatorial background.

In addition to this, the signal yield is limited by several intrinsic factors. The production cross-section of the Ω_c^0 is considerably lower than that of lighter charm hadrons, and the specific decay mode $\Omega_c^0 \rightarrow \Omega^- \pi^+ \pi^- \pi^+$ has a low branching fraction compared to more common two-body decays [7]. Moreover, reconstructing the full decay chain involves six charged particles, some originating from long-lived intermediate states such as the Λ^0 , which may decay outside the region covered by the vertex detector. This complicates track reconstruction and introduces further inefficiencies.

III. DECAY OF INTEREST

The decay process analyzed in this project involves the weak decay of the heavy-flavoured baryon Ω_c^0 into a final state composed of lighter hadrons. The decay chain can be expressed as:

$$\Omega_c^0 \rightarrow \Omega^- (\rightarrow \Lambda^0 (\rightarrow p \pi^-) K^-) \pi^+ \pi^- \pi^+$$

The final state consists of six charged particles and involves three separate decay vertices.

Excited Ω^- states are expected to decay strongly and promptly into a ground-state Ω^- and a pair of oppositely

charged pions. If such resonances are produced in the Ω_c^0 decay, they would appear as peaks in the invariant mass distribution of its decay products, the $\Omega^- \pi^+ \pi^-$ system.

Strange baryons have very long lifetimes as they mostly decay via the weak interaction. This is the case for our decay chain, which involves three distinct decay vertices. The primary decay, that of the Ω_c^0 , mainly decays within the VELO, as the Ω_c^0 has a mean lifetime of about $6.9 \times 10^{-14} \text{ s}$, which is relatively short but non-negligible. Consequently, the three pions directly resultant from that decay are always reconstructed as long tracks.

In contrast, almost all of the Λ^0 and many of the Ω^- will decay after the VELO, since they have significantly longer lifetimes, $2.6 \times 10^{-10} \text{ s}$ and $8.2 \times 10^{-11} \text{ s}$ respectively. As a consequence, the tracks from their decay products can be either long or downstream. Based on this, events are classified into three track type categories: LLL, DDL, DDD.

Each category has different advantages and limitations. In the LLL configuration, where all the decay products traverse the VELO, the tracking precision and vertex resolution are optimal. This leads to enhanced momentum measurements and mass resolution. However, this category suffers from reduced statistics due to the large lifetimes of Ω^- and Λ^0 . It also tends to suffer from increased combinatorial background, which arises from random combinations of unrelated particles produced at the primary vertex that are mistakenly reconstructed as Ω_c^0 candidates.

The DDD category, on the other hand, benefits from significantly lower combinatorial background, since downstream tracks are less likely to originate from unrelated prompt particles. This category provides a higher initial number of signal candidates, but the absence of VELO information limits the quality of the track reconstruction, resulting in degraded momentum and vertex resolution.

The DDL category provides an intermediate scenario: it retains improved resolution compared to DDD while maintaining a higher signal yield than LLL. Despite moderate background contamination, it preserves a substantial number of correctly reconstructed decays.

Given that the statistical analysis is ultimately limited by the number of available signal candidates, the categories DDL and DDD are combined in the present study. This approach increases the overall signal yield while keeping sufficient resolution.

The behavior of the momentum resolution for these different track types is further illustrated in Appendix A, where Figures 8, 9, and 10 present the signal mass distributions corresponding to each track category, highlighting the distinct momentum resolution differences in the reconstruction of the Ω^- baryon.

IV. CANDIDATES SELECTION

The initial dataset, obtained after the trigger and pre-selection stages, contains a large number of events. However, the background level is substantial, making it difficult to observe a clear signal in the invariant mass distribution of the reconstructed Ω_c^0 candidates. To isolate the signal, the mass of the Ω_c^0 is used as a discriminating observable. Signal events are expected to cluster around the known mass value of 2695.2 MeV/ c^2 [9], while background candidates form a smooth distribution.

In order to enhance the visibility of the signal and reduce the impact of combinatorial background, a set of selection criteria is applied. These requirements are based on variables that exhibit significant discriminating power between genuine decays and random combinations. The choice of variables is guided by physical knowledge of the decay topology.

One of the most effective observables for discrimination is the transverse momentum (p_T) of the final-state particles. Due to the relatively large mass of the Ω_c^0 , signal decays are expected to produce daughter particles with higher p_T than those originating from generic background processes. Accordingly, minimum thresholds on p_T are imposed on the Ω_c^0 candidate and on each of the pions in the final state.

Additional selection criteria are applied based on vertex quality. Signal decays tend to form well-defined secondary vertices, in contrast to background candidates, which typically exhibit poorer vertex fits. Variables such as the vertex fit quality χ_{vtx}^2 and the flight distance significance χ_{FD}^2 are used to reject poorly reconstructed combinations.

Further requirements are imposed on the impact parameter significance χ_{IP}^2 of the final-state tracks, which quantifies how inconsistent a particle's trajectory is with originating from the primary vertex. Signal particles from long-lived decays like the Ω_c^0 are expected to exhibit large χ_{IP}^2 values due to their displacement from the interaction point, whereas prompt background typically has low χ_{IP}^2 . A complete summary of the applied cuts is provided in Appendix B.

The effect of these selection criteria is illustrated in Figures 2, 3, and 4, which shows the invariant mass distribution of Ω_c^0 candidates after applying the full set of cuts for the DDD, DDL and combined (DDD+DDL) categories, respectively. In all distributions a clear peak is visible around the expected mass, indicating a significant signal contribution despite the remaining background. The similar shapes and characteristics of the signal and background components in the DDL and DDD distributions (Figures 2 and 3) further support their combination to increase the statistical power, as presented in Figure 4.

To provide context for the observed signal yield, the results are compared with previous measurements. For instance, Figure 5 displays an invariant mass distribution of Ω_c^0 from an earlier study [13], obtained through a similar analysis technique but using a different decay

channel, $\Omega_c^0 \rightarrow \Xi^- K^- \pi^+ \pi^+$. Since both analyses are based on the same Run 2 dataset, this comparison allows a meaningful evaluation of the relative branching ratios.

A direct comparison between the DDL invariant mass distributions from the present analysis (Figure 2) and the previous study (Figure 5) provides additional insight into the relative signal yields. While the earlier analysis was based on the decay $\Omega_c^0 \rightarrow \Xi^- K^- \pi^+ \pi^+$, which has a branching ratio of approximately 0.68, the current study focuses on the decay $\Omega_c^0 \rightarrow \Omega^- \pi^+ \pi^- \pi^+$, with a lower branching ratio of about 0.32 [7]. The observed number of signal candidates in the DDL category reflects this difference: 429 candidates are reconstructed in the present channel, compared to 886 in the previous one. Taking into account the ratio of branching fractions, the relative yields are consistent within expectations, indicating similar overall efficiencies and validating the reconstruction and selection strategy used in this analysis.

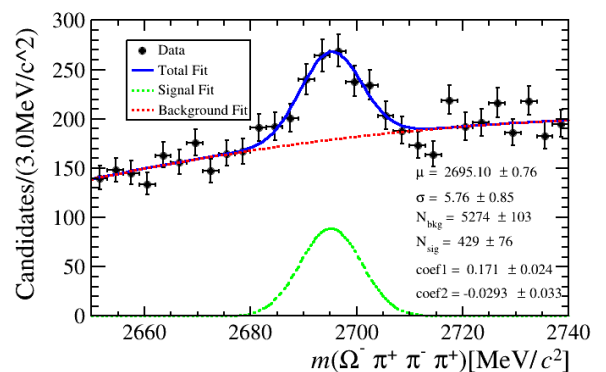


FIG. 2: Invariant mass distribution of Ω_c^0 candidates in the DDL track category, after applying all selection criteria.

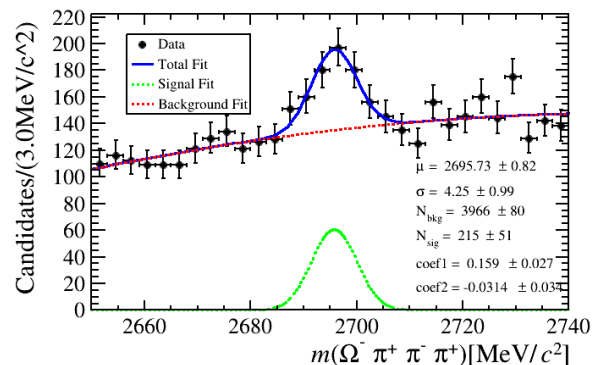


FIG. 3: Invariant mass distribution of Ω_c^0 candidates in the DDD track category, after applying all selection criteria.

To estimate the signal yield and quantify the background, the distribution is fitted with a model consisting of a Gaussian function to describe the signal peak and a second-order Chebyshev polynomial to account

for the combinatorial background [12]. The Gaussian component captures the resolution of the detector and the spread of the reconstructed signal around the nominal mass, while the Chebyshev polynomial models the smooth distribution of random combinations. The fit provides key information on the number of signal events, the resolution, and the overall purity of the sample.

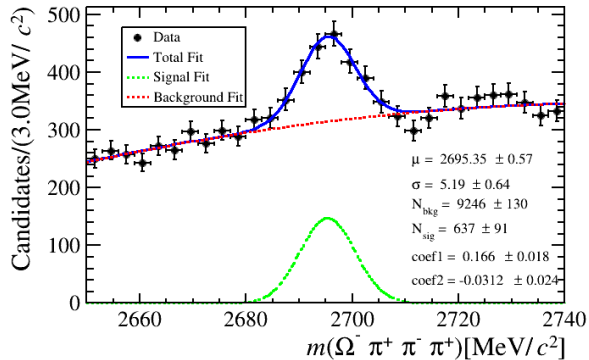


FIG. 4: Combined invariant mass distribution of Ω_c^0 candidates from the DDL and DDD track categories, after applying all selection criteria.

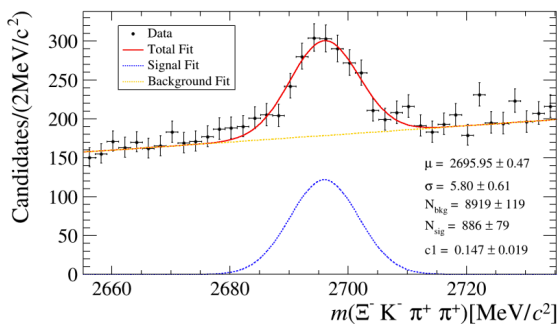


FIG. 5: Distribution of Ω_c^0 invariant mass candidates in the DDL category from the decay $\Omega_c^0 \rightarrow \Xi^- K^- \pi^+ \pi^+$, as obtained in [13]. Used for comparison with the current analysis based on the $\Omega^- \pi^+ \pi^- \pi^+$ channel.

V. OBTAINING SIGNAL DISTRIBUTIONS WITH THE *SPlot* METHOD

While the invariant mass of the Ω_c^0 offers a clean separation between signal and background, this is not the case for other kinematic variables of interest. Directly analyzing these variables without accounting for background contamination would result in distorted distributions. To overcome this issue, the *sPlot* technique [11] is used.

This method is based on a likelihood fit of the Ω_c^0 mass distribution, shown in Fig. 4, where the signal and background components are modeled using a Gaussian and

a second-order Chebyshev polynomial, respectively. The fit assigns each event a statistical weight, known as an *sWeight*, which reflects its probability of originating from the signal.

By applying these weights to the data, the contribution from background is statistically subtracted on an event-by-event basis. This allows the extraction of signal-only distributions for variables that are not too correlated with the invariant mass from the fit.

The analysis presented in the following sections uses these *sWeights* to study the invariant mass of $\Omega^- \pi^+ \pi^-$ combinations. This approach enables the identification of possible intermediate resonances, while suppressing the combinatorial background that would otherwise obscure such structures.

VI. FINAL RESULTS

To search for excited states of the Ω^- baryon, the invariant mass of the $\Omega^- \pi^+ \pi^-$ system is computed using the decay products of the reconstructed Ω_c^0 candidates. The Ω^- itself is reconstructed through its decay chain $\Omega^- \rightarrow \Lambda^0 K^-$, with $\Lambda^0 \rightarrow p \pi^-$.

Given the limited mass resolution of downstream tracks, the accuracy of the reconstructed Ω^- mass is improved by substituting the calculated Ω^- mass with its world-average value from the Particle Data Group (PDG), 1672.45 MeV/c² [9].

Since the decay of the Ω_c^0 includes three charged pions, and only two are expected to originate from a possible intermediate excited Ω^- state, there is an ambiguity in the pion pairing. To account for this, invariant mass spectra are constructed using both possible combinations of two pions together with the reconstructed Ω^- . These two spectra are shown in Figures 6 and 7, each weighted by the *sWeights* derived from the fit to the Ω_c^0 invariant mass distribution, as described in the previous section.

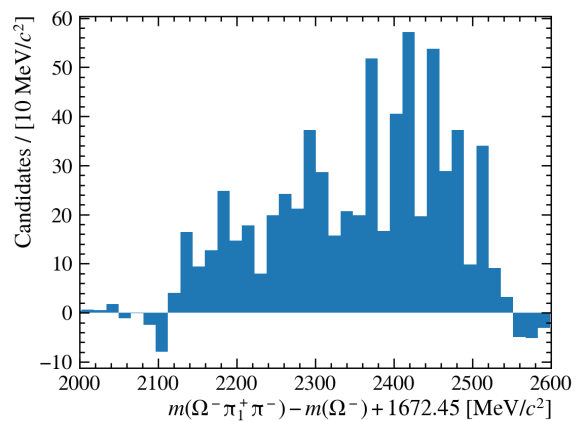


FIG. 6: Invariant mass spectrum of $\Omega^- \pi^+ \pi^-$ using one pion pairing, weighted with the *sWeights*. A mild enhancement is observed near 2470 MeV/c².

The two invariant mass distributions obtained from the different pions are not symmetric and display visibly distinct shapes. This discrepancy, combined with the limited number of signal events, significantly reduces the robustness of the analysis and prevents any definitive interpretation of the spectra.

Nevertheless, both distributions show an unusual structure between 2450 and 2500 MeV/c^2 compatible with the $\Omega^-(2470)$ resonance observed in past experiments.

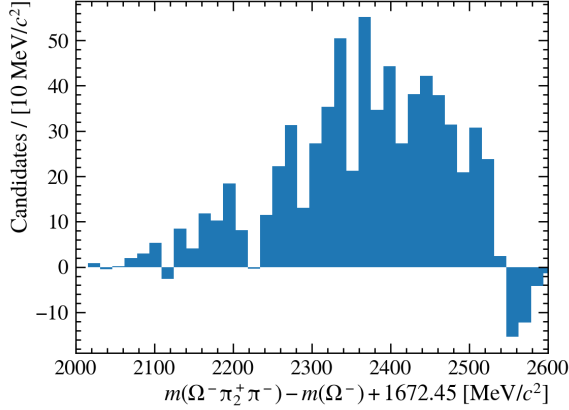


FIG. 7: Invariant mass spectrum of $\Omega^- \pi^+ \pi^-$ using the alternative pion pairing. Similar features are observed in the same mass region.

VII. CONCLUSIONS

This work presents a study of the resonance spectrum of the Ω^- baryon through the decay $\Omega_c^0 \rightarrow \Omega^- \pi^+ \pi^- \pi^+$, using data recorded by the LHCb experiment during Run 2.

A dedicated selection strategy was implemented to suppress combinatorial background and reconstruct Ω_c^0 candidates. To maximize the statistical yield while maintaining sufficient resolution, the DDL and DDD tracking categories were combined. The signal yield observed in the DDL category was compared to a previous study using a different decay channel [13], and found to be consistent with expectations based on relative branching fractions. This validates the reconstruction and selection strategy used in the present work.

After background subtraction using the *sPlot* technique, the invariant mass distributions of $\Omega^- \pi^+ \pi^-$ combinations show noticeable differences depending on the chosen pion pairing. These asymmetries, along with limited statistics, prevent a definitive interpretation of the results and need to be studied in future work.

Nonetheless, both spectra exhibit an unusual structure in the 2450–2500 MeV/c^2 region, loosely compatible with the known $\Omega^-(2470)$ resonance. While this excess may point to the presence of an excited state, the current dataset does not allow a conclusive identification, and background or reconstruction effects cannot be ruled out.

Further studies with increased statistics, refined selection strategies, and amplitude analysis techniques will be essential to confirm or discard the presence of excited Ω^- states in this decay channel.

Acknowledgments

I express my sincere gratitude to my supervisors, Carla Marin Benito and Lukas Calefice, for their expert guidance, feedback, and support throughout the development of this project, carried out within the framework of the LHCb experiment at CERN.

-
- [1] V.E.Barnes *et al.*, Observation of a Hyperon with Strangeness-3, *Phys. Rev. Lett.* **12**, 204 (1964), 10.1103/PhysRevLett.12.204.
 - [2] S. F. Biagi *et al.*, First observation of Ω^* resonances, *Z. Phys. C* **31**, 33–39 (1986), KEK-Preprint-8601068.
 - [3] D. Aston *et al.*, Observation of Ω^{*-} production in $K^- p$ interactions at 11 GeV/c , *Phys. Lett. B* **194**, 579–584 (1987), SLAC-PUB-4132.
 - [4] D. Aston *et al.*, Observation of a new Ω^{*-} at 2.47 GeV/c^2 in $K^- p$ interactions at 11 GeV/c , *Phys. Lett. B* **215**, 799–804 (1988), SLAC-PUB-4657.
 - [5] Belle Collaboration, J. Yelton *et al.*, Observation of an excited Ω^- baryon, *Phys. Rev. Lett.* **121**, 052003 (2018), arXiv:1805.09384.
 - [6] LHCb Collaboration, R. Aaij *et al.*, Observation of excited Ω_c^0 baryons in $\Omega_b^- \rightarrow \Xi_c^+ K^- \pi^-$ decays, *Phys. Rev. D* **110**, 032001 (2024), arXiv:2502.18063.
 - [7] J.Yelton *et al.*, Measurement of branching fractions of hadronic decays of the Ω_c^0 baryon, *Phys. Rev. D* **97**, 032001 (2018), 10.1103/PhysRevD.97.032001.
 - [8] T. Chen and C. Guestrin, XGBoost: A scalable tree boosting system, in *Proceedings of the 22nd ACM SIGKDD Conference* (2016), arXiv:1910.10322.
 - [9] Particle Data Group, S. Navas *et al.*, Review of Particle Physics, *Phys. Rev. D* **110**, 030001 (2024), 10.1103/PhysRevD.110.030001.
 - [10] LHCb Collaboration, The LHCb Detector at the LHC, *JINST* **3**, S08005 (2008), LHCb-DP-2008-001.
 - [11] M. Pivk and F. R. Le Diberder, *sPlot: a statistical tool to unfold data distributions*, *Nucl. Instrum. Meth. A* **555**, 356–369 (2005), arXiv:physics/0402083.
 - [12] ROOT Data Analysis Framework, Documentation of the class *RooChebychev*, *RooChebychev*.
 - [13] C. Garcia Gazulla, *Multi-strange baryon spectroscopy at the LHCb experiment in $\Omega_c^0 \rightarrow \Xi^- K^- \pi^+ \pi^+$ decays*, CERN-THESIS-2024-308, cds.cern.ch/record/2921782.

Selecció d'esdeveniments per espectroscòpia de barions en l'experiment LHCb al
decaïment $\Omega_c^0 \rightarrow \Omega^- \pi^+ \pi^- \pi^+$

Author: Albert Casamitjana Formiga

Facultat de Física, Universitat de Barcelona, Diagonal 645, 08028 Barcelona, Spain.

Advisor: Carla Marín Benito and Lukas Calefice

Resum: Aquest projecte investiga l'espectre de ressonàncies del barió Ω^- mitjançant el decaïment $\Omega_c^0 \rightarrow \Omega^- \pi^+ \pi^- \pi^+$, utilitzant dades del Run 2 de l'experiment LHCb. S'ha aplicat una selecció específica per suprimir el fons i reconstruir candidats a Ω_c^0 , i s'han combinat les categories de traça DDL i DDD per augmentar el rendiment del senyal. Per a la substracció del fons s'ha utilitzat el mètode *sPlot*. Els espectres de massa invariable de $\Omega^- \pi^+ \pi^-$ mostren diferències segons la combinació de pions, i l'estadística limitada impedeix extreure una interpretació concloent.

Paraules clau: Física de partícules, física d'altres energies, anàlisi de dades, partícules estranyes, espectroscòpia

ODS: Indústria, innovació i infraestructures

Appendix A: Track types

Figures 8, 9 and 10 show the invariant mass distributions of Ω^- candidates for the LLL, DDL, and DDD categories, respectively. These distributions illustrate the impact of tracking configuration on mass resolution.

The Gaussian width (σ) of the Ω^- mass peak increases progressively from 2.0686 MeV/ c^2 in the LLL sample, to 2.7195 MeV/ c^2 in DDL, and 3.324 MeV/ c^2 in DDD. This confirms that the absence of VELO information leads to degraded track reconstruction quality. In particular, the DDD distribution deviates from a clear Gaussian shape and appears significantly broadened, with a flatter signal component that blends into the background. This reflects the limited momentum and vertex resolution associated with downstream-only tracks, which impacts the precision in reconstructing long-lived baryons such as the Ω^- .

These results highlight the importance of the track configuration in determining the sensitivity to narrow resonant structures in the invariant mass spectrum.

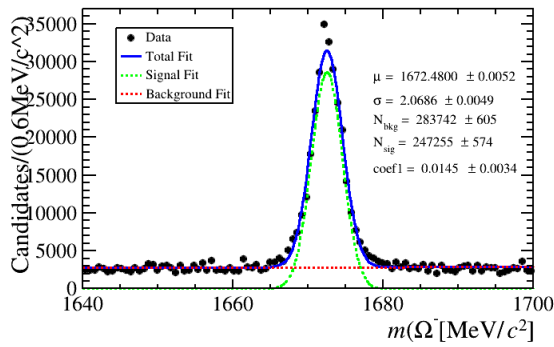


FIG. 8: Invariant mass distribution of Ω^- candidates in the LLL category.

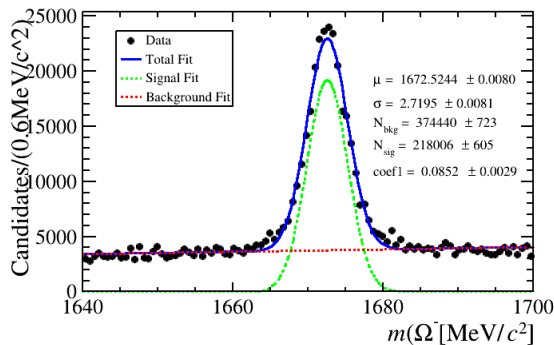


FIG. 9: Invariant mass distribution of Ω^- candidates in the DDL category.

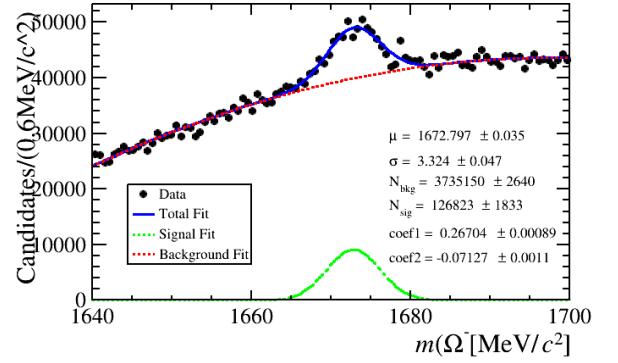


FIG. 10: Invariant mass distribution of Ω^- candidates in the DDD category.

In addition, while these distributions reflect the resolution degradation of the Ω^- when reconstructed using only DDL or DDD tracks, this effect becomes less relevant in the full Ω_c^0 reconstruction. As can be seen in Figures 2 and 3, where the Ω^- is combined with three additional long tracks from the pions, the overall resolution is dominated by those long tracks. As a result, the resolution is no longer strictly correlated with the tracking category of the Ω^- candidate. This reduces the impact of the degraded resolution from the downstream Ω^- reconstruction, especially when the known Ω^- mass is subtracted from the full invariant mass. However, the effect is not entirely negligible, as in this case, the DDL category exhibits slightly worse resolution than DDD, indicating that other factors beyond tracking category may influence the final invariant mass resolution, such as vertex constraints or correlation with the additional tracks.

Appendix B: Selection criteria

Table I provides a selection of cuts for various variables, applied to enhance the signal significance and suppress background. These include kinematic thresholds, vertexing quality, displacement from the primary vertex, particle identification requirements, and invariant mass consistency with known values.

Variable	Selection criteria
$p_T(\Omega_c^0)$	$> 1500 \text{ MeV}/c$
$p_T(\pi_1^+)$	$> 350 \text{ MeV}/c$
$p_T(\pi_2^+)$	$> 350 \text{ MeV}/c$
$p_T(\pi^-)$	$> 350 \text{ MeV}/c$
$\max(p_T(\pi_1^+, \pi_2^+, \pi^-))$	$> 400 \text{ MeV}/c$
$\chi_{\text{vtx}}^2(\Omega_c^0)$	< 9
$\chi_{\text{FD}}^2(\Omega_c^0)$	> 15
$\chi_{\text{FD}}^2(\Omega^-)$	> 30
$\min(\chi_{\text{IP}}^2(\pi_1^+, \pi_2^+, \pi^-))$	> 3
$\max(\chi_{\text{IP}}^2(\pi_1^+, \pi_2^+, \pi^-))$	> 3
$\rho(\Omega_c^0)$	$> 0.1 \text{ mm}$
$\Delta\rho(\Omega^-, \Omega_c^0)$	$> 0.1 \text{ mm}$
$\Delta\rho(\Lambda^0, \Omega^-)$	$> 0.05 \text{ mm}$
$\cos(\vartheta_{\text{DIRA}})(\Omega_c^0)$	> 0.9999
$z_{\text{vtx}}(\Lambda^0) - z_{\text{vtx}}(\Omega^-)$	> 0
$z_{\text{vtx}}(\Omega^-) - z_{\text{vtx}}(\Omega_c^0)$	> 0
$\text{ProbNN}\pi(\pi_1^+) \cdot (1 - \text{ProbNNK}(\pi_1^+))$	> 0.4
$\text{ProbNN}\pi(\pi_2^+) \cdot (1 - \text{ProbNNK}(\pi_2^+))$	> 0.4
$\text{ProbNN}\pi(\pi^-) \cdot (1 - \text{ProbNNK}(\pi^-))$	> 0.4
$\text{GhostProb}(\pi_1^+)$	< 0.3
$\text{GhostProb}(\pi_2^+)$	< 0.3
$\text{GhostProb}(\pi^-)$	< 0.3
$ m(\Omega^-) - m_{\text{PDG}}(\Omega^-) $	$< 15 \text{ MeV}/c^2$
$ m(\Lambda^0) - m_{\text{PDG}}(\Lambda^0) $	$< 10 \text{ MeV}/c^2$

TABLE I: Selection criteria applied to the dataset.